Calculation of energy subband structures of corrugated lateral-surface superlattices based on variational principles

1996 J. Phys.: Condens. Matter 8 7605

(http://iopscience.iop.org/0953-8984/8/41/009)

J. Phys.: Condens. Matter **8** (1996) 7605–7617. Printed in the UK

Calculation of energy subband structures of corrugated lateral-surface superlattices based on variational principles

Hong Sun†, Jin-Min Huang‡ and Kin-Wah Yu§

† Department of Physics and Institute of Condensed Matter Physics, Shanghai Jiao Tong University, Shanghai 200030, People's Republic of China

‡ Shanghai Vocational College of Mechanical and Electrical Engineering, Branch II, Shanghai 200082, People's Republic of China

§ Department of Physics, The Chinese University of Hong Kong, Shatin, New Territories, Hong Kong

Received 27 March 1996, in final form 5 July 1996

Abstract. A theoretical method is developed for calculating energy subbands of carriers in lateral-surface superlattices with corrugated interfaces (CLSSLs). Based on the variational principle and a coordinate transformation, the method overcomes difficulties in constructing wave functions which must satisfy complicated boundary conditions on corrugated interfaces. The method is tested numerically via calculations of electron subbands, probability distributions and intersubband optical absorptions of CLSSLs with periodic variations of well thicknesses. Sensitive dependencies of electron subbands, probability distributions and intersubband optical absorptions on structural parameters of CLSSLs are predicted.

1. Introduction

Much attention is currently being devoted to two-dimensional electronic systems with further periodic confinements of carriers (electrons and holes) along lateral directions [1–20]. In the literature, these systems are often referred to as lateral-surface superlattices (LSSLs). A variety of interesting electronic and optical phenomena associated with energy subband structures of LSSLs have been discovered experimentally. Of the various structures of LSSLs proposed, the one produced by direct crystal growth methods without using lithographic techniques offers great potential for wide applications in microelectronics and optoelectronics, for lithographic techniques usually introduce defects and produce samples with lateral dimensions ($>$100 nm) much larger than their vertical dimensions ($\approx$10 nm) [2, 12, 14, 17]. Some of the direct growth methods include deposition of AlAs and GaAs fractional layers on (001) vicinal surfaces of GaAs substrates [4, 11] and direct molecular-beam epitaxy growth of GaAs and AlAs layers on high-index GaAs surfaces [20]. Lateral confinements of carriers in these systems are achieved due to periodically corrugated interfaces separating well and barrier materials, creating corrugated lateral-surface superlattices (CLSSLs) with lateral periods ranging from 3 to 30 nm. Strong periodic lateral confinements (or equivalently, lateral periodic potentials) imposed on carriers introduce new energy subband structures with subband gaps large enough to induce novel physical properties in CLSSLs.

Calculations of energy subbands of CLSSLs have been carried out by several groups [21–24]. Due to complicated boundary conditions on corrugated interfaces, these calculations

0953-8984/96/417605+13$19.50

rely on numerical methods, such as the tight-binding [21, 22] or finite-element methods [23], which require very heavy computer work. For more complicated problems, such as exciton states in CLSSLs, calculations involve either even heavier numerical work or oversimplified assumptions [25]. In this paper, we propose a numerical method for calculating energy subbands of CLSSLs based on the variational principle, which requires much less computer work compared with the tight-binding or finite-element methods. The basic idea of the method is to introduce a coordinate transformation which transforms CLSSLs to ordinary quantum wells with planar interfaces and effective lateral periodic potentials arising from corrugated interfaces. The coordinate transformation was introduced in our previous paper where we calculated electron subbands for CLSSLs with infinitely high potential barriers on interfaces or with finite barriers but neglecting the difference of electron effective mass between well and barrier materials of CLSSLs [26, 27]. Our present calculations show that both of these approximations are not very good for the GaAl/AlAs CLSSLs in which we are interested. In the present paper, the method is extended to include the effect of mass difference between well and barrier materials and to calculations of valence subbands of GaAl/AlAs CLSSLs. As we shall explain later, the inclusion of the mass difference in the theory is not trivial. The method can also be easily extended to other low-dimensional electronic systems with non-regular interfaces, such as quantum-well wires with interface profiles deviated from rectangular or cylindrical structures and quantum dots with interface profiles deviated from cubic or sphere structures.

The paper is organized as follows. The general theory is presented in the next section. The accuracy of the method is tested numerically via calculations of electron subbands for GaAs/AlAs CLSSL structures. The results and discussions are given in the final section.

2. Theory

The CLSSL that we considered consists of the GaAs well and AlAs barriers separated by interfaces at $z_\pm = \pm L_z/2 + f_\pm(x)$, where L_z is the average thickness of the well and $f_\pm(x)$ describe the profile of the corrugated interfaces. In the effective-mass approximation, the Hamiltonian for the carrier (the electron or hole) in the CLSSL can be written generally as

$$H = \begin{pmatrix} T_{11} & \cdots & T_{1n} \\ \vdots & & \vdots \\ T_{n1} & \cdots & T_{nn} \end{pmatrix} + IV(\boldsymbol{r}) \tag{1}$$

with

$$T_{ij} = \sum_{\alpha\beta} \frac{\partial}{\partial x_\alpha} \gamma_{\alpha\beta}^{(ij)} \frac{\partial}{\partial x_\beta} \qquad (\alpha, \beta = x, y, z; i, j = 1, \ldots, n) \tag{2}$$

where I is a unit matrix and $V(\boldsymbol{r})$ is the band offset for conduction or valence bands between bulk GaAs and AlAs materials. The hermiticity of the Hamiltonian requires $T_{ji}^\dagger = T_{ij}$, and so $\gamma_{\beta\alpha}^{(ji)*} = \gamma_{\alpha\beta}^{(ij)}$. By comparing H with Hamiltonians of electrons and holes obtained in the literature, we obtain the parameters $\gamma_{\alpha\beta}^{(ij)}$, a large part of which are zeros. If a single-band model is used for electrons, we have $\gamma_{\alpha\beta}^{(ij)}(\boldsymbol{r}) = -\gamma\delta_{\alpha\beta}\delta_{i,1}\delta_{j,1}$, where γ is inversely proportional to the electron effective mass in the CLSSL. If the Hamiltonian for holes is obtained from the Luttinger Hamiltonian [28] by replacing $\gamma_i k_\alpha k_\beta$ with the symmetrized operator

$$-\frac{1}{2}\left(\frac{\partial}{\partial x_\alpha}\gamma_i\frac{\partial}{\partial x_\beta} + \frac{\partial}{\partial x_\beta}\gamma_i\frac{\partial}{\partial x_\alpha}\right)$$

where γ_i $(i = 1, 2, 3)$ are the Luttinger parameters of the well and barrier materials of the CLSSL, we have $\gamma_{\alpha\beta}^{(ij)} = \gamma_{\beta\alpha}^{(ij)}$. If the Hamiltonian of holes is derived from the exact envelope-function equations developed by Burt [29], generally we have $\gamma_{\alpha\beta}^{(ij)} \neq \gamma_{\beta\alpha}^{(ij)}$ [30].

The eigen-wave function of the carrier is written as a vector

$$\Psi(\boldsymbol{r}) = \begin{pmatrix} \psi_1(\boldsymbol{r}) \\ \vdots \\ \psi_n(\boldsymbol{r}) \end{pmatrix} \tag{3}$$

which satisfies the following eigenvalue equation:

$$H\Psi(\boldsymbol{r}) = E\Psi(\boldsymbol{r}). \tag{4}$$

The boundary condition of Ψ is determined by the continuity of the wave function, and the continuity of the probability current density at each interface, the latter of which is obtained by integrating equation (4) over a small cylinder across the interface. We have that the following quantities must be continuous at each interface:

$$\psi_i\big|_{\text{continuous}} \qquad \text{and} \qquad \sum_{j=1}^{n}\sum_{\alpha\beta}\gamma_{\alpha\beta}^{(ij)}\frac{\partial\psi_j}{\partial x_\beta}n_\alpha\bigg|_{\text{continuous}} \qquad (i = 1, \ldots, n) \tag{5}$$

with $\boldsymbol{n} = (n_x, n_y, n_z)$ the unit vector normal to the interface at each point. Making use of the boundary condition equation (5), it is easy to show that the Hamiltonian defined in equations (1) and (2) is hermitian. Equations (4) and (5) form the complete set of equations which determine subband energies and wave functions of the carrier in the CLSSL.

For a quantum well with planar interfaces parallel to the xy-plane, the boundary condition at each interface reduces to

$$\psi|_{\text{continuous}} \qquad \text{and} \qquad \frac{1}{m_e}\frac{\partial\psi}{\partial z}\bigg|_{\text{continuous}} \tag{6}$$

for the electron if a single-band model is used, and to that given in reference [30] for the hole if the Hamiltonian is derived from the exact envelope-function equations.

The above eigenvalue problem can also be formulated based on the following variational principle: if the wave function Ψ (equation (3)) makes the first-order difference of the following functional:

$$L[\Psi] = \sum_{ij=1}^{n} L_{ij}[\psi_i^*, \psi_j] - E\sum_{i=1}^{n}\int \mathrm{d}\boldsymbol{r}\ \psi_i^*\psi_i \tag{7}$$

equal to zero, where

$$L_{ij}[\psi_i^*, \psi_j] = -\sum_{\alpha\beta}\int \mathrm{d}\boldsymbol{r}\ \frac{\partial\psi_i^*}{\partial x_\alpha}\gamma_{\alpha\beta}^{(ij)}\frac{\partial\psi_j}{\partial x_\beta} + \delta_{ij}\int \mathrm{d}\boldsymbol{r}\ V(\boldsymbol{r})\psi_i^*\psi_j \tag{8}$$

then ψ_i $(i = 1, \ldots, n)$ must satisfy the eigenvalue equation (4) and (*natural*) boundary condition equation (5). The only exceptional case is when the barrier potential goes infinitely high. The boundary condition of Ψ reduces to

$$\psi_i = 0 \qquad (i = 1, \ldots, n) \tag{5$'$}$$

at each interface. The wave function Ψ must be so constructed that it makes $\delta L[\Psi] = 0$ and meanwhile satisfies the (*essential*) boundary condition equation (5′).

To find an appropriate complete set of functions for expanding the wave functions ψ_i $(i = 1, \ldots, n)$, which must satisfy the boundary condition equation (5′) when the barrier potential goes infinitely high, we introduce the following coordinate transformation [26, 27]:

$$\begin{aligned} \tilde{x} &= x \\ \tilde{y} &= y \\ \tilde{z} &= L_z\{z - [f_+(x) + f_-(x)]/2\}/[L_z + f_+(x) - f_-(x)] \end{aligned} \tag{9}$$

which transforms the CLSSL in space $\boldsymbol{r}$ to a quantum well with planar interfaces at $\tilde{z}_\pm = \pm L_z/2$ in space $\tilde{\boldsymbol{r}}$, as shown in figure 1. In the transformed space $\tilde{\boldsymbol{r}}$, the functional $L[\Psi]$ can be written as

$$\tilde{L}[\tilde{\Psi}] = L_0[\tilde{\Psi}] + \delta L[\tilde{\Psi}] \tag{10}$$

where $L_0[\tilde{\Psi}]$ is the corresponding functional for a quantum well with planar interfaces, and $\delta L[\tilde{\Psi}]$ can be explained as an effective periodic lateral potential arising from the corrugated interfaces. In space $\tilde{\boldsymbol{r}}$, the wave function $\tilde{\Psi}(\tilde{\boldsymbol{r}})$ is expanded using the eigen-wave functions of the corresponding quantum well, which form a complete set:

$$\begin{aligned} \tilde{\psi}^{(i)}_{n\boldsymbol{k}}(\tilde{\boldsymbol{r}}) &= \sum_{lm} A^{(i)}_{lm}(n, \boldsymbol{k})\zeta^{(i)}_l(\tilde{z})\frac{\mathrm{e}^{\mathrm{i}[(k_x - Q_m)\tilde{x} + k_y\tilde{y}]}}{\sqrt{S_0}} \\ &= \sum_{lm} A^{(i)}_{lm}(n, \boldsymbol{k})\varphi^{(i)}_{lm}(\tilde{\boldsymbol{r}}, \boldsymbol{k}) \qquad (i = 1, \ldots, n) \end{aligned} \tag{11}$$

where S_0 is the surface area of the CLSSL, $\boldsymbol{k}$ is the in-plane wave vector of the carrier limited within the first Brillouin zone (FBZ), $Q_m = 2\pi m/L_x$ $(m = 0, \pm 1, \pm 2, \ldots)$ is the reciprocal-lattice wave vector associated with the lateral period L_x of the CLSSL and $\zeta^{(i)}_l(\tilde{z})$ is the ith component of the lth eigen-wave function of the quantum well in the $\tilde{z}$-direction. If the barrier potential height is infinite, $\zeta^{(i)}_l(\tilde{z})$ approaches zero on the interfaces. And so Ψ satisfies the (*essential*) boundary condition equation (5′). The summation $\sum_l$ in equation (11) should in principle include all the wave functions of $\zeta^{(i)}_l(\tilde{z})$, which for finite barriers consist of localized states (l discrete) and extended states (l continuous). The numerical results in the next section show that for the GaAs/AlAs CLSSL in which we are interested, it is sufficient to consider only the localized states in the expansion of $\tilde{\psi}^{(i)}_{n\boldsymbol{k}}(\tilde{\boldsymbol{r}})$ in equation (11) for low-energy subbands. Substituting $\tilde{\psi}^{(i)}_{n\boldsymbol{k}}(\tilde{\boldsymbol{r}})$ into $\tilde{L}[\tilde{\Psi}]$, and differentiating it with respect to the expansion coefficients $A^{(i)}_{lm}(n, \boldsymbol{k})$, we obtain the following equation which determines the energy subbands of carriers in the CLSSL:

$$\det \| L_{ilm,jl'm'}(\boldsymbol{k}) - E_n(\boldsymbol{k}) J_{ilm,jl'm'}(\boldsymbol{k}) \| = 0 \tag{12}$$

where $L_{ilm,jl'm'}(\boldsymbol{k}) = \tilde{L}_{ij}[\varphi^{(i)*}_{lm}(\tilde{\boldsymbol{r}}, \boldsymbol{k}), \varphi^{(j)}_{l'm'}(\tilde{\boldsymbol{r}}, \boldsymbol{k})]$ is defined by equation (8) with the integration coordinates (x, y, z) transformed to $(\tilde{x}, \tilde{y}, \tilde{z})$ by equation (9), and

$$J_{ilm,jl'm'}(\boldsymbol{k}) = \delta_{ij} \int \mathrm{d}\tilde{\boldsymbol{r}}\ J(\tilde{\boldsymbol{r}})\varphi^{(i)*}_{lm}(\tilde{\boldsymbol{r}}, \boldsymbol{k})\varphi^{(j)}_{l'm'}(\tilde{\boldsymbol{r}}, \boldsymbol{k}) \tag{13}$$

with $J(\tilde{\boldsymbol{r}}) = [f_+(\tilde{x}) - f_-(\tilde{x})]/L_z$ the Jacobian determinant associated with the coordinate transformation.

The variational principle simplifies the numerical calculation by dealing with only first derivatives of the wave functions and satisfying the (*natural*) boundary condition equation (5) automatically at each interface. For cases where the (*essential*) boundary condition equation (5′) is required, the coordinate transformation makes it easy to find the appropriate variational wave function by transforming the CLSSL to a quantum well with planar interfaces. If one starts the numerical calculation from the Hamiltonian, as we did

in our previous papers [26, 27], the trial wave function Ψ must be constructed to satisfy the boundary condition equation (5) in order to make the Hamiltonian hermitian. It is easy to show by direct differentiation that even for electron states, the boundary condition equation (5) in space $\tilde{\boldsymbol{r}}$ after the coordinate transformation does not take the same simple form as that for a quantum well with planar interfaces, unless the electron mass difference between the well and barrier materials is neglected or the barrier potential is infinitely high. For general cases, where the mass difference is considered, it is still difficult to construct trial wave functions which satisfy the (*transformed*) boundary condition in space $\tilde{\boldsymbol{r}}$. It becomes even more difficult to construct trial wave functions for hole states which satisfy the complicated boundary condition on corrugated interfaces of the CLSSL. The difficulty due to the boundary condition is avoided in the present theory based on the variational principle. In the next section, the method outlined above is applied to calculations of electron subbands for GaAs/AlAs CLSSLs, where we will show that the coordinate transformation reduces considerably the calculated number of matrix elements in equation (12) for the CLSSL in which we are interested.

3. Electron states in CLSSLs

For electrons in conduction bands of GaAs/AlAs CLSSLs, the parameters $\gamma_{\alpha\beta}^{(ij)}$ which determine the functional $L[\Psi]$ defined in equations (7), (8) are given by

$$\gamma_{\alpha\beta}^{(ij)}(\boldsymbol{r}) = -\frac{\hbar^2}{2m_e(\boldsymbol{r})}\delta_{\alpha\beta}\delta_{i,1}\delta_{j,1} \tag{14}$$

if a single-band model is used, where $m_e(\boldsymbol{r})$ describes the electron effective mass in the GaAs well ($m_{\mathrm{GaAs}} = 0.0665m_0$) and AlAs barriers ($m_{\mathrm{AlAs}} = 0.124m_0$). The conduction band offset $V_c(\boldsymbol{r})$ is $V_c = 0$ in the well and $V_c = 1.06$ eV in the barriers. In most of the CLSSL examples reported in the literature, one of interfaces of the CLSSL is step shaped with a step height equal to 2.83 Å [4, 5]. Because electrons are confined mainly in the centre of the well, the effect of these monolayer steps on electrons can be neglected by taking one of the interfaces as a plane. We assume that the interface profile of the CLSSL, $z_\pm = \pm L_z/2 + f_\pm(x)$, is given within one period ($-L_x/2 < x < L_x/2$) by

$$f_-(x) = 0$$

$$f_+(x) = \begin{cases} \delta L_z\{1 - (2|x|/L_w)^{\alpha_1}\} & 0 \leqslant |x| \leqslant L_w/2 \\ -\delta L_z\{1 - [(L_x - 2|x|)/(L_x - L_w)]^{\alpha_2}\} & L_w/2 < |x| \leqslant L_x/2 \end{cases} \tag{15}$$

with δL_z and L_x the amplitude and lateral period of the interface corrugation. L_w gives the length of the CLSSL where the well thickness is larger than the average thickness L_z, that is $f_+(x) > 0$. α_1, $\alpha_2 > 1$ and are related to each other by $\alpha_1/\alpha_2 = L_w/(L_x - L_w)$, which ensures that $f_+(x)$ and its derivative are continuous at each point. If α_1, $\alpha_2 \to \infty$, we have an ideal square-well-shaped corrugated interface. In figure 1(a), we give the interface profile of a GaAs/AlAs CLSSL with $L_z = 7$ nm, $\delta L_z = 2$ nm, $L_x = 15$ nm, $L_w = L_x/2$ and $\alpha = \alpha_1 = \alpha_2 = 30$. The interface profile of the CLSSL after the coordinate transformation in space $\tilde{\boldsymbol{r}}$ is shown in figure 1(b).

We first set $k_y = 0$ in the calculation. The numerical calculation of equation (12) is carried out by limiting the infinite expansion of $\tilde{\Psi}_{n\boldsymbol{k}}(\tilde{\boldsymbol{r}})$ in equation (11) to $l = 1, 2, \ldots, L_0$ and $m = 0, \pm1, \pm2, \ldots, \pm M_0$. The matrix elements in equation (12) are written as

$$L_{lm,l'm'}(k_x) = (k_x - Q_m)(k_x - Q_{m'})L_{lm,l'm'}^{(1)} + (k_x - Q_m)L_{lm,l'm'}^{(2)} + (k_x - Q_{m'})L_{lm,l'm'}^{(3)} + L_{lm,l'm'}^{(4)} \tag{16}$$

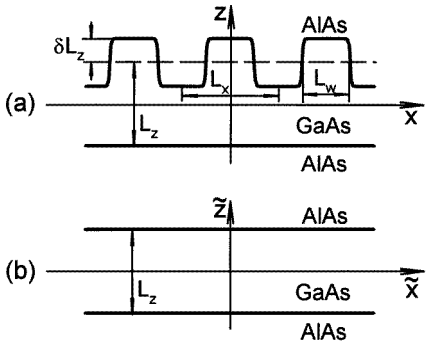

Figure 1. (a) The profile of the GaAs/AlAs CLSSL considered in the text in space $\boldsymbol{r}$ with structural parameters $L_z = 7$ nm, $\delta L_z = 2$ nm, $L_x = 15$ nm, $L_w = 7.5$ nm and $\alpha = \alpha_1 = \alpha_2 = 30$. (b) The profile of the CLSSL in the transformed space $\tilde{\boldsymbol{r}}$ after the coordinate transformation.

Table 1. Numerical results for electron subband energies $E_n(k_x)$ in the GaAs/AsAl CLSSL with the structural parameters $L_z = 7$ nm, $\delta L_z = 2$ nm, $L_x = 15$ nm $L_w = 7.5$ nm and $\alpha = \alpha_1 = \alpha_2 = 50$. The calculation is carried out at the centre ($k_x = 0$) and edge ($k_x = Q/2$) of the FBZ. $L_0 \times (2M_0 + 1)$ expansion wave functions are used in the calculation. The unit of the energy is meV.

$k_x/Q = 0.0$	$E_0(k_x)$	$E_1(k_x)$	$E_2(k_x)$	$E_3(k_x)$	$E_4(k_x)$
$L_0 = 1, M_0 = 10$	137.6	230.3	379.1	518.5	771.5
$L_0 = 2, M_0 = 10$	129.7	216.9	303.3	323.2	489.7
$L_0 = 3, M_0 = 10$	126.6	213.2	301.7	311.7	483.8
$L_0 = 4, M_0 = 10$	125.7	213.0	298.1	310.4	478.8
$L_0 = 4, M_0 = 7$	128.1	215.0	299.7	321.1	481.6
$L_0 = 4, M_0 = 8$	127.2	214.2	299.1	317.6	480.4
$L_0 = 4, M_0 = 9$	126.4	213.7	298.4	314.0	480.0
$L_0 = 4, M_0 = 10$	125.7	213.0	298.1	310.4	478.8
$k_x/Q = 0.5$	$E_0(k_x)$	$E_1(k_x)$	$E_2(k_x)$	$E_3(k_x)$	$E_4(k_x)$
$L_0 = 1, M_0 = 10$	138.7	225.8	399.2	486.5	840.2
$L_0 = 2, M_0 = 10$	132.3	205.9	294.6	376.7	433.8
$L_0 = 3, M_0 = 10$	129.6	200.4	291.2	370.7	423.7
$L_0 = 4, M_0 = 10$	128.6	200.3	287.9	368.6	423.1
$L_0 = 4, M_0 = 7$	130.6	204.5	290.3	373.6	432.6
$L_0 = 4, M_0 = 8$	129.9	202.9	289.5	371.8	429.1
$L_0 = 4, M_0 = 9$	129.3	201.6	288.7	370.2	425.9
$L_0 = 4, M_0 = 10$	128.6	200.3	287.9	368.6	423.1

where $L^{(p)}_{lm,l'm'}$ $(p = 1, \ldots, 4)$ is independent of k_x. We also notice from equation (13) that $J_{lm,l'm'}(k_x) = J_{lm,l'm'}$ is independent of k_x. The subscripts (i, j) in $L_{ilm,jl'm'}(k_x)$ and $J_{ilm,jl'm'}$ are dropped since for the electron $i = j = 1$. Once the matrices $J_{lm,l'm'}$ and $L^{(p)}_{lm,l'm'}$ are determined, the subband energies $E_n(k_x)$ at any k_x can be calculated from equation (12) by standard programs. Due to the simple interface profile of the CLSSL in the transformed space $\tilde{\boldsymbol{r}}$ (see figure 1(b)), integrations over $\tilde{x}$ and $\tilde{z}$ in $J_{lm,l'm'}$ and $L^{(p)}_{lm,l'm'}$ are separable. We

have

$$J_{lm,l'm'} = J^{x}_{m,m'}\, J^{z}_{l,l'} \qquad L^{(p)}_{lm,l'm'} = L^{x,(p)}_{m,m'} L^{z,(p)}_{l,l'} \qquad (p = 1, \ldots, 4). \tag{17}$$

Instead of $5 \times [(L_0N_0)^2 + L_0N_0]/2$ (with $N_0 = 2M_0 + 1$) *two*-dimensional integrations, only $5 \times (L_0^2 + L_0 + N_0^2 + N_0)/2$ *one*-dimensional integrations need to be calculated, where the hermiticity of the matrices has been taken into consideration. If $L_0 = 4$ and $M_0 = 10$, instead of 17 850 *two*-dimensional integrations, only 1205 *one*-dimensional integrations need to be calculated, which saves greatly on computer time. All of the numerical calculations given in this paper were performed on an IBM PC/486. The numerical calculation for a typical figure or table takes about 10 minutes.

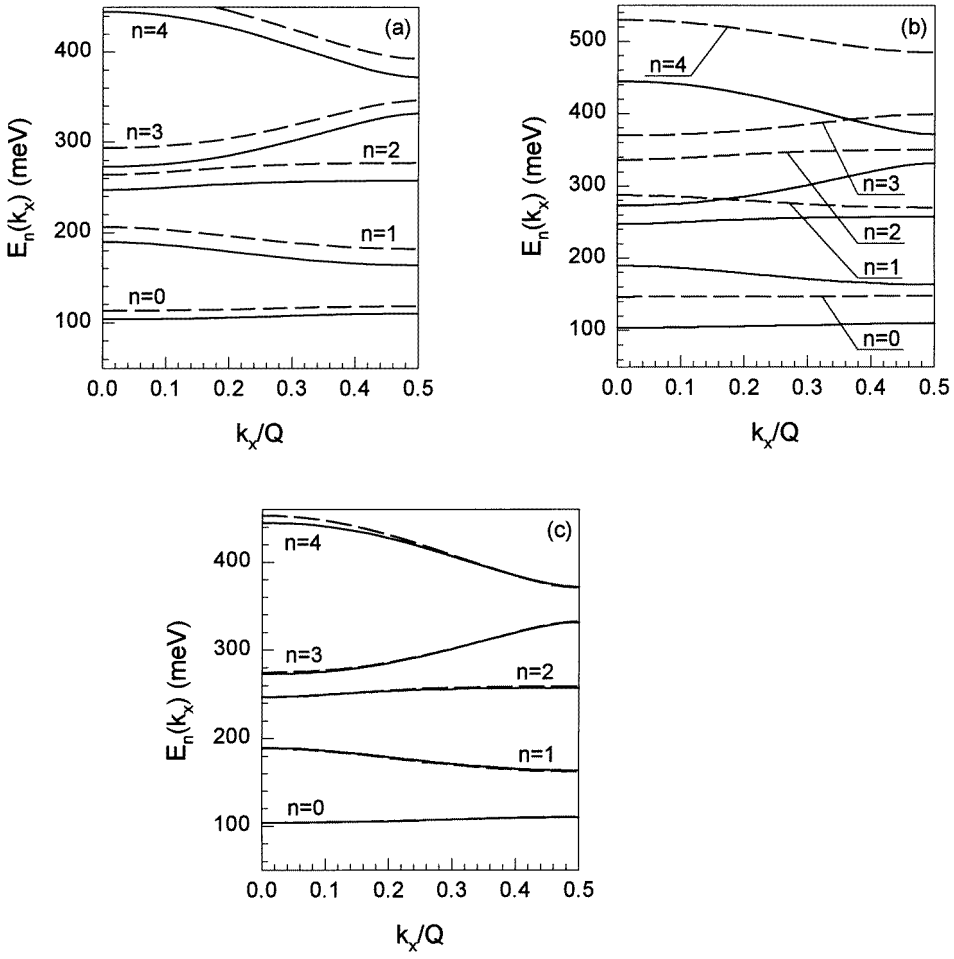

Figure 2. Electron subband energies $E_n(k_x)$ (the solid lines) as functions of the reduced wave vector k_x/Q for the same GaAs/AlAs CLSSL as that in figure 1. Also given are subband energies $E_n(k_x)$ calculated for the same CLSSL with the difference of the electron effective mass neglected by taking $m_{\mathrm{AlAs}} = m_{\mathrm{GaAs}} = 0.0665m_0$ (the dashed lines in (a)), with the height of the barrier potential assumed to be infinite (the dashed lines in (b)) and with $k_y = Q$ (the dashed lines in (c)). We set $k_y = 0$ in all calculations except for that of the dashed lines in (c).

In table 1, we give the calculated results for the first few subband energies at the centre ($k_x = 0$) and edge ($k_x = Q/2$ with $Q = 2\pi/L_x$) of the FBZ for different L_0 and M_0. The structural parameters of the GaAs/AlAs CLSSL are the same as those in figure 1. The numerical error is expected to be 1% if $L_0 = 4$ and $M_0 = 10$.

In figure 2, we give the calculated subband energies $E_n(k_x)$ (the solid lines) as functions of the reduced wave vector k_x/Q for the same GaAs/AlAs CLSSL as that in figure 1. Also given in figure 2 are the subband energies $E_n(k_x)$ for the same CLSSL but with the difference of the electron effective mass neglected by taking $m_{\mathrm{AlAs}} = m_{\mathrm{GaAs}} = 0.0665m_0$ (the dashed lines in (a)) and with the height of the barrier potential assumed to be infinite (the dashed lines in (b)). The results show that both of these approximations, especially the latter, are not very good for the GaAs/AlAs CLSSLs that we considered. For cases where $k_y \neq 0$, due to the translational symmetry along the y-direction of the CLSSL, the subband energy of the electron can be written as

$$E_n(k_x, k_y) = \frac{\hbar^2 k_y^2}{2m_{GaAs}} + E_n(k_x) \tag{18}$$

if the difference between the effective masses of the well and barriers is neglected. When the mass difference is not negligible, we can write $E_n(k_x, k_y)$ formally as that in equation (18). But now $E_n(k_x)$ is determined by a k_y-dependent band offset:

$$V_{eff}(\boldsymbol{r}, k_y) = V(\boldsymbol{r}) + \frac{\hbar^2 k_y^2}{2m_{\mathrm{GaAs}}}\left[\frac{m_{\mathrm{GaAs}}}{m_e(\boldsymbol{r})} - 1\right]. \tag{19}$$

In calculations carried out in this paper, k_y is limited to $|k_y| < Q$. In figure 2(c), we show the calculated results for $E_n(k_x)$ with $k_y = 0$ (the solid lines) and $k_y = Q$ (the dashed lines) for the same CLSSL. It is obvious that when $|k_y| < Q$, the dependence of $E_n(k_x)$ on k_y can be neglected.

The exact interface profile of the CLSSL depends on the growth condition. It has been found experimentally that during growth, Ga and Al migrate laterally between the regions of AlAs bars [4] (see figure 1(a)). The actual interface profile deviates from that of an ideal square well. To investigate the effect of structures of CLSSLs on energy subbands, in figure 3 we give the calculated results of the electron subband direct transition energy $\Delta E_n(k_x) = E_n(k_x) - E_0(k_x)$ at $k_x = 0$ (the dashed lines) and $k_x = Q/2$ (the solid lines), and subband width $WE_n = \max\{E_n(k_x)\} - \min\{E_n(k_x)\}$ (the chain lines) as functions of (a) the structural parameter $\alpha = \alpha_1 = \alpha_2$, (b) the lateral period L_x and (c) the average thickness L_z for GaAs/AlAs CLSSLs with other structural parameters being the same as those in figure 1. The transition energy $\Delta E_n(k_x)$ and subband width WE_n approach constants as $\alpha \to \infty$, corresponding to those for the ideal square-well corrugation. When α is below 50, $\Delta E_n(k_x)$ and WE_n depend sensitively on the exact interface profile of the CLSSL. The direct transition energy $\Delta E_n(k_x)$ and subband width WE_n determine mainly peak positions and widths of far-infrared (FIR) optical absorptions of CLSSLs associated with electron transitions between different electron subbands. By changing structural parameters (α, L_z, L_x etc), one is able to adjust FIR absorption spectra of CLSSLs.

The probability distribution of the electron in the CLSSL is given in figure 4, where the normalized electron wave function $|\psi_{nk_x}(x, z)|^2$ is plotted in the original space $\boldsymbol{r}$ as functions of x and z for (a) $n = 0$, (b) $n = 1$ and (c) $n = 2$ with $k_x = Q/2$. The structural parameters of the CLSSL are the same as those in figure 1. The electron probability distribution satisfies the periodic condition $|\psi_{n\boldsymbol{k}}(x + L_x, z)|^2 = |\psi_{n\boldsymbol{k}}(x, z)|^2$. Electrons in the ground state $\psi_{0\boldsymbol{k}}(\boldsymbol{r})$ concentrate mainly in parts of the GaAs well where the well is thick (see also figure 1). While the electron distribution in the excited states is rather complicated. In the

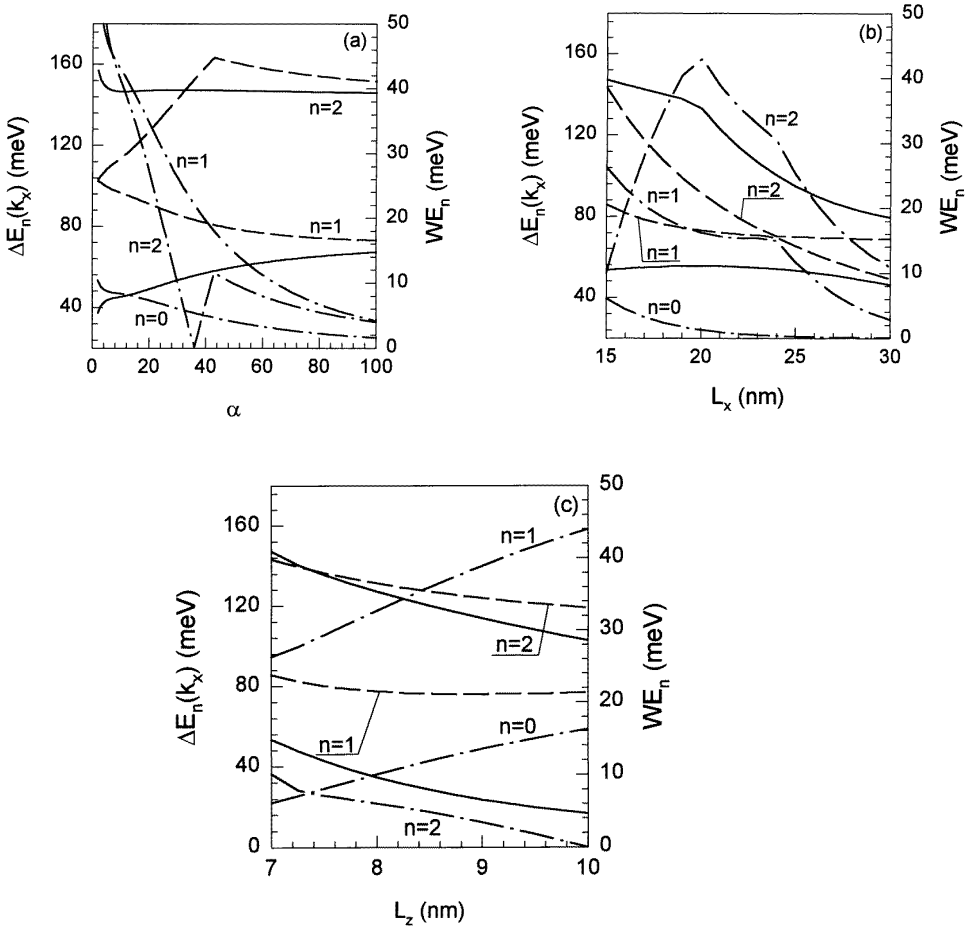

Figure 3. The electron intersubband direct transition energy $\Delta E_n(k_x)$ at $k_x = 0$ (the dashed lines) and $k_x = Q/2$ (the solid lines), and subband width WE_n (the chain lines) as functions of (a) the structural parameter $\alpha = \alpha_1 = \alpha_2$, (b) the lateral period L_x and (c) the average thickness L_z of the GaAs/AlAs CLSSLs with other structural parameters being the same as those in figure 1.

first excited state $\psi_{1\boldsymbol{k}}(\boldsymbol{r})$, no node is found in the electron probability distribution along the z-direction, which leads to a small transition matrix $\langle\psi_{0\boldsymbol{k}}(\boldsymbol{r})|p_z|\psi_{1\boldsymbol{k}}(\boldsymbol{r})\rangle$ connecting the ground and first excited states. In the second excited state $\psi_{2\boldsymbol{k}}(\boldsymbol{r})$, no node is found along the x-direction, which leads to a small transition matrix $\langle\psi_{0\boldsymbol{k}}(\boldsymbol{r})|p_x|\psi_{2\boldsymbol{k}}(\boldsymbol{r})\rangle$ connecting the ground and second excited states. For incident light polarized in direction α ($\alpha = x, y, z$), FIR optical absorptions associated with electron transitions between electron subbands are proportional to the square of the transition matrix $|\langle\psi_{0\boldsymbol{k}}(\boldsymbol{r})|p_\alpha|\psi_{n\boldsymbol{k}}(\boldsymbol{r})\rangle|^2$. Strong anisotropic FIR optical absorptions are expected for the CLSSLs that we considered.

In figure 5, we give the calculated imaginary parts of the dielectric function ϵ_2, associated with electron intersubband transitions, as functions of the energy of incident light $\hbar\omega$ for the same CLSSL as that in figure 1. The polarization of incident light is in the x-direction (the chain lines) and in the z-direction (the solid lines). The electron density

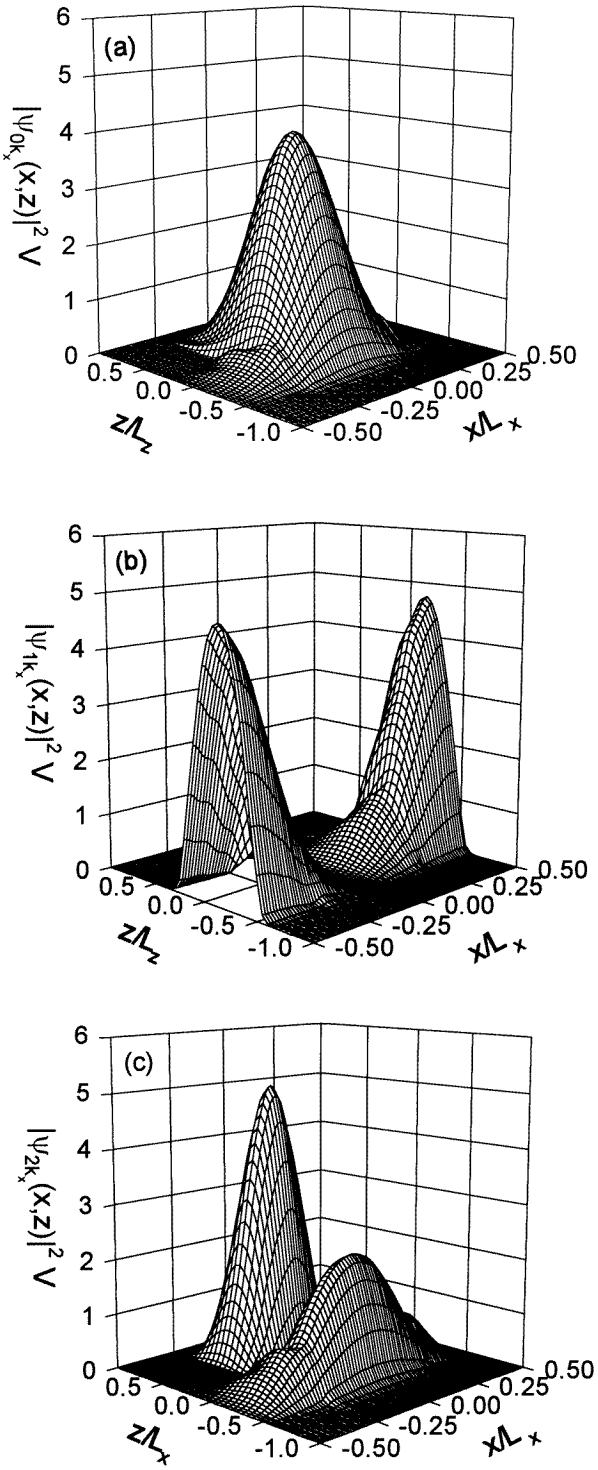

Figure 4. The distributions of the electron probability $|\Psi_{nk_x}(x,z)|^2$ plotted in the original space $\boldsymbol{r}$ as functions of x and z for (a) $n = 0$, (b) $n = 1$ and (c) $n = 2$ with $k_x = Q/2$. The structural parameters of the CLSSL are the same as those in figure 1. V is the average volume of the CLSSL.

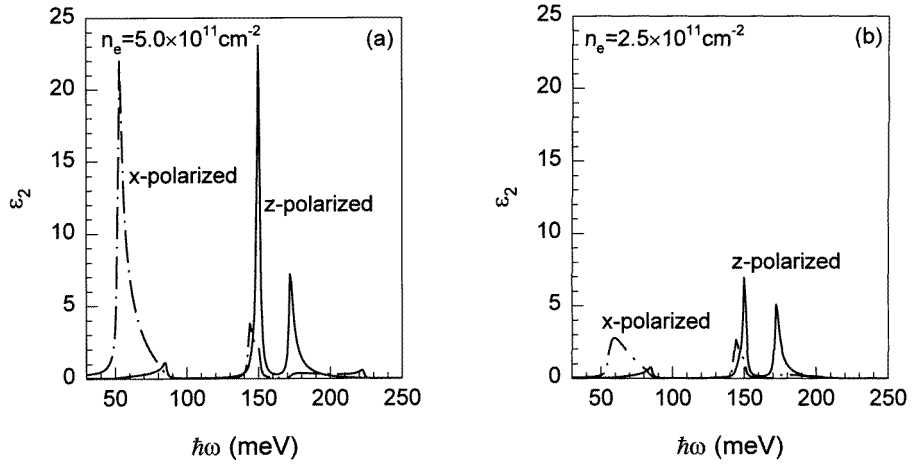

Figure 5. The calculated imaginary parts of the dielectric function ϵ_2 as functions of the energy of incident light $\hbar\omega$ for the same CLSSL as that in figure 1. The polarization of incident light is in the x-direction (the chain lines) and z-direction (the solid lines). The electron density is (a) $n_e = 5.0 \times 10^{11}$ cm^{-2} at which the Fermi energy level is pushed into the first minigap of the electron subbands, and (b) $n_e = 2.5 \times 10^{11}$ cm^{-2} at which the Fermi energy level remains in the first subband.

is (a) $n_e = 5.0 \times 10^{11}$ cm^{-2} at which the Fermi energy level is pushed into the first minigap of the electron subbands, and (b) $n_e = 2.5 \times 10^{11}$ cm^{-2} at which the Fermi energy level remains in the first subband. The results in figure 5(a) show that for incident light polarized in the x-direction, the strong FIR absorption is due to electron transitions between the ground and first excited states, and for incident light polarized in the z-direction, it is determined by electron transitions between the ground and second excited states, consistent with the electron probability distributions obtained in figure 4. To be more specific, the electron transitions mainly responsible for strong FIR absorptions are those near the edge of the FBZ with $k_x \approx Q/2$ (see also figure 2). Results in figure 5(b) show that when the electron density is low and the states near the edge of the FBZ are not occupied, strong FIR absorption peaks disappear. This carrier-density-dependent absorption behaviour makes the CLSSLs that we considered here suitable for designing the so-called carrier-activated modulators, which was first suggested using conventional quantum wells [31, 32]. Due to the transitional symmetry in directions parallel to planar interfaces of quantum wells, intersubband absorptions are non-zero only when incident light is polarized perpendicular to quantum wells. In particular, intersubband absorptions vanish in quantum wells for normal incident light. But for the CLSSLs that we considered here, intersubband absorptions exist even for normal incident light.

In figure 6, we give the calculated electron density n_e (the solid line) as a function of the Fermi energy E_F for the same CLSSL as that in figure 1. Also shown in figure 6 is the calculated Fermi wave vector k_F (the chain line) defined by $E_F = E_0(k_F)$. The dashed line in figure 6 indicates the Fermi energy level at which the first subband is filled up with electrons.

Electron redistributions (see figure 4) caused by corrugated interfaces of CLSSLs will induce static electric potentials (the electron screening effect) which always tend to compensate effective potentials due to corrugated interfaces. As the electron density

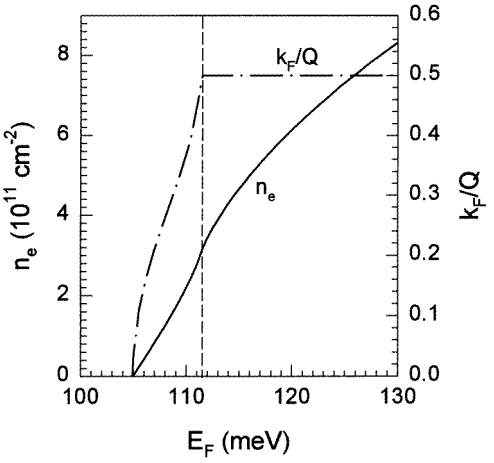

Figure 6. The calculated electron density n_e (the solid line) and Fermi wave vector k_F (the chain line) as functions of the Fermi energy E_F for the same CLSSL as that in figure 1. The dashed line indicates the Fermi energy level at which the first subband is filled up with electrons.

increases, the strength of the lateral potential and so also electron subband gaps will decrease due to the increase of the electron screening effect. In a previous paper, we found that the effect of (*intersubband*) plasmons on FIR absorptions of CLSSLs, which causes blue-shifts of FIR absorption peaks, is negligible for CLSSLs with lateral periods L_x less than 15 nm [33]. It is expected that the total effect on FIR absorptions caused by the increase of the electron density is red-shifts of FIR absorption peaks. The detailed study of the electron screening effect on FIR absorptions of CLSSLs based on self-consistent calculations will be given elsewhere.

4. Conclusions

We have developed a theoretical method for calculating energy subbands of carriers in lateral-surface superlattices with corrugated interfaces. Based on the variational principle and a coordinate transformation, the method overcomes difficulties in constructing wave functions which must satisfy complicated boundary conditions on corrugated interfaces. The method is tested numerically via calculations of electron subbands, electron probability distributions and FIR intersubband absorptions for CLSSLs with periodic variations of well thicknesses. Sensitive dependences of electron subbands, electron probability distributions and FIR absorptions on structural parameters of CLSSLs are predicted, and these will find potential applications in novel device designs in microelectronics and optoelectronics.

Acknowledgments

This work was supported by the National Natural Science Foundation of China and the Science and Technology Foundation of High Education of China. K W Yu acknowledges the financial support by the Research Grants Council of the Hong Kong Government under project number 461/95P.

References

[1] Petroff P M, Gossard A G and Wiegmann W 1984 *Appl. Phys. Lett.* **45** 620
[2] Warren A C, Antoniadis D A, Smith H I and Melngailis J 1985 *IEEE Electron. Device Lett.* **6** 294
[3] Fukui T and Saito H 1987 *Appl. Phys. Lett.* **50** 824
[4] Tanaka M and Sakaki H 1988 *Japan. J. Appl. Phys.* **27** L2025
[5] Fukui T and Saito H 1988 *J. Vac. Sci. Technol.* B **6** 1373
[6] Gaines J M, Petroff P M, Kroemer H, Simes R J, Geels R S and English J H 1988 *J. Vac. Sci. Technol.* B **6** 1478
[7] Motohisa J, Tanaka M and Sakaki H 1989 *Appl. Phys. Lett.* **55** 1214
[8] Weiss D, von Klitzing K, Ploog K and Weimann G 1989 *Europhys. Lett.* **8** 117
[9] Gerhardts R R, Weiss D and von Klitzing K 1989 *Phys. Rev. Lett.* **62** 1173
[10] Winkler R W and Kotthaus J P 1989 *Phys. Rev. Lett.* **62** 1177
[11] Tsuchiya M, Gaines J M, Yan R H, Simes R J, Holtz P O, Coldren L A and Petroff P M 1989 *Phys. Rev. Lett.* **62** 466
[12] Ismail K, Chu W, Yen A, Antoniadis D A and Smith H I 1989 *Appl. Phys. Lett.* **54** 460
[13] Tanaka M and Sakaki H 1989 *Appl. Phys. Lett.* **54** 1326
[14] Kohl M, Heitmann D, Grambow P and Ploog K 1990 *Phys. Rev.* B **42** 2941
[15] Sugawara H, Schulman J H and Sakaki H 1991 *J. Appl. Phys.* **69** 2722
[16] Stormer H J, Pfeiffer L N, Baldwin K W, West K W and Spector J 1991 *Appl. Phys. Lett.* **58** 726
[17] Kern K, Demel T, Heitmann D, Grambow P, Zhang Y H and Ploog K 1991 *Superlatt. Microstruct.* **9** 11
[18] Smoliner J, Rosskopf V, Berthold G, Gornik E, Böhm G and Weimann G 1992 *Phys. Rev.* B **45** 1915
[19] Fukui T, Tsubaki K, Saito H, Kasu M and Honda T 1992 *Surf. Sci.* **267** 588
[20] Nötzel R, Ledentsov N N and Ploog K 1992 *Phys. Rev.* B **45** 3507
[21] Citrin D S and Chang Y C 1991 *Phys. Rev.* B **43** 11 703
[22] Jouanin C and Bertho D 1994 *Superlatt. Microstruct.* **16** 229
[23] Leng M H and Lent C S 1994 *Phys. Rev.* B **50** 10 823
[24] Kiselev A A and Rössler U 1994 *Phys. Rev.* B **50** 14 283
[25] Glutsch S and Bechstedt F 1993 *Phys. Rev.* B **47** 6385
[26] Sun H 1992 *Phys. Rev.* B **46** 12 371
[27] Dai W K and Sun H 1992 *J. Phys.: Condens. Matter* **5** L263
[28] Luttinger J M 1956 *Phys. Rev.* **102** 1030
[29] Burt M G 1992 *J. Phys.: Condens. Matter* **4** 6651
[30] Foreman B A 1993 *Phys. Rev.* B **48** 4964
[31] Johnson N F, Ehrenreich H and Jones R V 1988 *Appl. Phys. Lett* **53** 180
[32] Johnson N F, Ehrenreich H, Hui P M and Yong P M 1990 *Phys. Rev.* B **41** 3655
[33] Sun H and Yu K W 1996 *Phys. Lett.* A **218** 105